SACLANTCEN MEMORANDUM
serial no.: SM-273

SACLANT UNDERSEA RESEARCH CENTRE

MEMORANDUM

VOLUME 1 OF 2

Measurements for satellite validation made from the RV Alliance during October and November 1991

P.J. Minnett

August 1993

Page count for SM-273 (excluding Covers and Data Sheet)

Pages	Total
i–vii	7
1–261	261
	268

SACLANT Undersea Research Centre
Viale San Bartolomeo 400
19138 San Bartolomeo (SP), Italy

tel: 0187 540 111
fax: 0187 524 600
telex: 271148 SACENT I

NORTH ATLANTIC TREATY ORGANIZATION

SACLANTCEN SM-273

Measurements for satellite validation made from the RV Alliance during October and November 1991

P.J. Minnett

The content of this document pertains to work performed under Project 23 of the SACLANTCEN Programme of Work. The document has been approved for release by The Director, SACLANTCEN.

Issued by:
Underwater Research Division

H. Urban
Division Chief

intentionally blank page

Measurements for satellite validation made from the RV Alliance during October and November 1991

P.J. Minnett

Executive Summary: This memorandum presents measurements of marine surface meteorology, sea-surface temperature and atmospheric profiles taken from the RV *Alliance* between 1 October and 9 November, 1991. These are to be used to study the accuracy with which sea-surface temperature and atmospheric precipitable water can be measured by infrared and microwave radiometers on earth observation satellites.

The measurements were taken on passage from Amsterdam to La Spezia, during two short instrument trials cruises, and on a non-interference basis during the cruise SPG 1/91 in the western Mediterranean Sea.

The calibrated measurements of sea and air temperatures, relative humidity, and long- and short-wave downwelling surface radiation are presented here as time series, beginning at about 1500Z on October 1 and continuing until about 1900Z on November 8, with the exceptions of days when the ship was in port at La Spezia. True winds, net long-wave surface radiation flux, and the turbulent air–sea exchanges of sensible and latent heat have been calculated and are presented. Profiles of atmospheric temperature and humidity are also displayed, and the ship's track is given in a graphical form.

This data report also serves to record the environmental conditions in which the other activities on the *Alliance* took place.

intentionally blank page

SACLANTCEN SM-273

Measurements for satellite validation made from the RV Alliance during October and November 1991

P.J. Minnett

Abstract: Measurements of sea-surface temperature, surface meteorology and atmospheric profiles were taken from the RV *Alliance* between 1 October and 9 November 1991. During this time the ship sailed from Amsterdam to La Spezia and then was deployed in the western Mediterranean Sea. The measurements are presented in graphical form, and daily statistics are given as tables. True winds, net long-wave radiation and turbulent air–sea fluxes have been calculated and are also presented. The measurements were made for application to studies of the accuracies of the retrieval of sea-surface temperature and atmospheric precipitable water from satellite radiometers.

Keywords: air–sea interaction ○ English Channel ○ Mediterranean Sea ○ meteorology ○ NE Atlantic Ocean ○ sea surface temperature

Contents

Acknowledgements: The measurements were taken as part of a collaborative effort between scientists of the Applied Oceanography Group of the SACLANT Undersea Research Centre (Dr. H.-H. Essen of the Satellite Remote Sensing Project), and Dr. P.J. Minnett of the Oceanographic and Atmospheric Sciences Division of the Brookhaven National Laboratory. The support of the technicians of the Ocean Engineering Department, and of the Digital Computing Department, as well as the at-sea support from the Captain and crew of

the *Alliance*, is gratefully acknowledged. The assistance of Kate Stansfield in preparing many of the figures and tables is also gratefully acknowledged.

The author was funded by the United States Department of Energy under Contract No. DE-AC02-7CH00016, with some support from the National Oceanographic and Atmospheric Administration (NA26GP0266-01).

1 Purpose

The measurements presented here were taken to provide data with which to make direct comparisons with the measurements of sea-surface temperature (SST) and the atmospheric water vapour burden (sometimes referred to as the precipitable water, PW) made from satellites. The satellite measurements are those of the operational Advanced Very High Resolution Radiometer (AVHRR) on the NOAA (National Oceanic and Atmospheric Administration) series of polar orbiting satellites, the operational Special Sensor Microwave Imager (SSM/I) on the DMSP (Defense Meteorological Satellite Program) series of polar orbiters, and the experimental Along-Track Scanning Radiometer on the polar obiter ERS-1 (ESA First Remote Sensing satellite) of the European Space Agency (ESA). The *in situ* measurements were taken from the NATO RV *Alliance* in the eastern Atlantic Ocean and western Mediterranean Sea.

The measurements can also be used to confirm the results of atmospheric radiative transfer models used to simulate the satellite measurements for the purpose of algorithm development (e.g. Llewellyn-Jones et al., 1984) or for the study of the theoretical error characteristic of satellite measurements (e.g. Minnett, 1986; 1990).

Furthermore the ship-borne measurements provide data for the study of the oceanic thermal skin effect (e.g. Robinson et al., 1984; Schluessel et al., 1987), by which the exchange of heat between the ocean and the atmosphere causes a temperature difference between the radiative temperature of the sea surface and that measured in the bulk of the water.

These measurements are complimentary to those taken during a cruise of the RV *Alliance* in June 1990 in a collaborative experiment, called the Mediterranean Aircraft–Ship Transmission Experiment (MASTEX), with the Meteorological Research Flight of the UK Meteorological Office (Minnett and Saunders, 1989; Saunders and Minnett, 1990; Minnett, 1992).

2
Background

Measurements of sea-surface variables from instruments on earth satellites are of great importance in oceanographic and climate change studies. In particular the large data sets generated by operational satellites offer an unrivalled description of pertinent variables on a global scale. In particular the AVHRR SST measurements, which now span more than a decade, are of great potential. A critical step in the data processing to retrieve SST from the satellite infrared measurements is in accounting for the effects of the intervening atmosphere. This is done by combining collocated measurements taken at different wavelength intervals (or channels) according to a simple algorithm. The precise form of the algorithm, or the coefficients used in an algorithm, can be determined by either comparing large sets of simultaneous satellite and *in situ* measurements (e.g. Strong and McClain, 1984) or by numerical simulations of the passage through the atmosphere of the radiation detected by the satellite radiometer (e.g. Minnett, 1986; 1990). Satellite measurements from which SST values can be derived are usually taken in the infrared part of the electromagnetic spectrum (although some measurements have been successfully made with those detecting microwave radiation), in spectral intervals where the atmosphere is relatively transparent. One such 'atmospheric window', at ~10–12 μm wavelengths, roughly coincides with the peak of the Planck function at temperatures typical of the sea-surface, and channels 4 and 5 of the AVHRR share this 'window'. The main component of atmospheric effects in this spectral interval is that due to water vapour, which exhibits so-called continuum absorption and emission, and this has a wavelength dependence across the window, being stronger at longer wavelengths. The appropriate combination of satellite measurements at these wavelengths can compensate, to a large degree, for the atmospheric effects. However, one of the main uncertainties is the description of the correct behaviour of the atmospheric water-vapour continuum (e.g. Grant, 1990), and shortcomings in its specification in radiative transfer models is a significant source of uncertainty in the numerical simulations and the resulting SST retrieval algorithms.

An alternative approach to the atmospheric correction in satellite SST retrievals, is to measure twice the infrared radiation at the satellite height arriving from the sea surface, each time through a different atmospheric path length. This is the measurement principal of the ATSR, which employs a conical scan mechanism to make measurements of the radiation leaving the sea surface with emission angles close to zero and close to 55°. In addition it makes multi-channel measurements at the same spectral intervals as the AVHRR. It also takes microwave measurements, but only at nadir, from which the PW can be calculated.

Broad swath (~1400 km) measurements of PW are made by the SSM/I, and these can be validated by direct comparison with the PW values derived from the ship-launched radiosondes.

3
Itinerary

The ship sailed from Amsterdam at about mid-day on October 1. The route from Holland was through the English Channel, across the Bay of Biscay, southward to the west of Portugal and through the Strait of Gibraltar, and across the Western Mediterranean to La Spezia. We ran into a severe storm during the night of October 1, which caused the ship to loose several hours' headway. Furthermore, the development of an inexplicable vibration of the propeller shafts caused a brief diversion to La Coruña for an underwater inspection by divers. No fouling was seen and the problem was solved by the ship's engineers en route.

The ship was in the port at La Spezia from the 9 to 15 October, 18 October, and 21 to 24 October to change over other equipment between cruises. The two short cruises on 16–17 October, and 19–20 October were in waters near to La Spezia, while the final cruise from 25 October to 9 November was divided between the Corsican Sea to the south of the island of Elba, and the western Mediterranean Sea to the west of Sardinia.

The track of the ship for the period 1 October to 9 November is shown in Fig. 1.

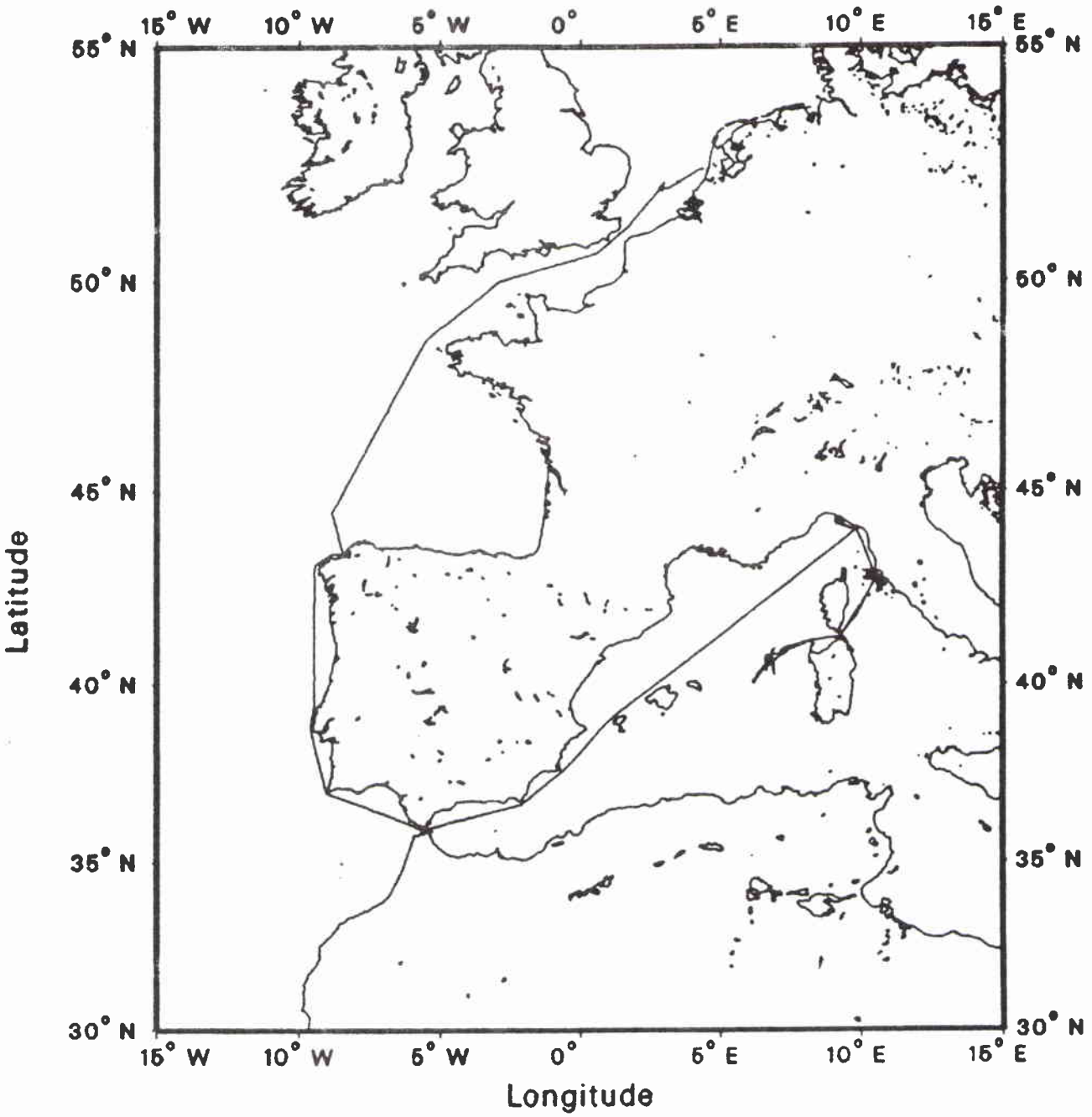

Figure 1 *A track plot of the position of the RV Alliance for the period covered by this report. The ship sailed from Amsterdam on October 1, arriving in La Spezia on October 9. Daily track plots are given in Appendix A.*

4

Ship-Board Instrumentation

For very nearly all of the period at sea, high quality measurements of sea-surface temperature, surface meteorological variables and surface infrared radiances were taken by a set of instruments mounted on the ship and logged by computers. The ship is equipped with a set of meteorological sensors (including SST thermometers) and a precision infrared SST radiometer and these were augmented by a sky radiometer and a radiosonde station for this cruise.

4.1. SURFACE METEOROLOGICAL VARIABLES

The system for measuring surface meteorological and oceanographic variables is called the ZAN (ZENO Alliance Network). This measures surface meteorological and oceanographic variables using various instruments distributed about the ship, the characteristics of which are given in Table 1. The sensors are sampled by remote 'Intelligent Sensor Interfaces' (ISIs), where calibration coefficients are applied and where mean values of measurements are calculated and stored before being transmitted to a central computer on a fibre-optic LAN (Fig. 2). A fuller description of the system is given by Reynolds et al. (1988).

The wind speed and direction were measured by R.M. Young anemometers (propeller and wind-vane type) mounted on the foremast, at a height of about 16 m above the water-line, and on a 7 m lattice-work mast at the stern of the ship, bringing the sensors to a height of about 12 m. The foremast carries two identical sensors to provide redundancy in case of failure and the three sets of sensors together ensure good measurements from all directions irrespective of the relative wind direction. Air temperature and humidity are also measured by precision thermistors and 'Rotronics hygromer' sensors at the same locations as the wind speed and direction. Again there are two sets of sensors at the foremast and one at the stern. Also mounted on the foremast are two radiometers, manufactured by the Eppley Laboratory, one to measure the downwelling short-wave insolation and the second to measure the downwelling long-wave radiation. The radiometers were not gimballed and therefore their measurements are subject to contamination by ship roll and pitch. This effect is believed to be small as MacWhorter and Weller (1991) have shown that, for the short-wave case at least, the drop in signal is less than 10% for amplitudes of rocking $< 35°$. Angles of pitch and roll were much less than this.

All of the sensors attached to the ZAN were sampled during this cruise at 1 Hz and a 1-min block average was generated at intervals of generally 2 min.

Table 1 *Characteristics of the RV Alliance sensors*[1]

Variable	Sensor Type	Units	Resolution	Accuracy	Comments
Sea surface temperature	Self-calibrating infrared radiometer	°C	0.05	0.2	Skin temperature
Sea surface temperature	Precision thermistor	°C	0.1	0.1	data from a depth of ~10 cm
Sea surface temperature	Precision thermistor	°C	0.01	0.01	data from a depth of 3 m
Sky temperature	Radiometer	°C	0.1	0.5	
Air temperature	Precision thermistor	°C	0.1	0.2	
Relative humidity	Hygristor	%	0.1	2.0	
Wind speed anemometer	Propeller	$m\ s^{-1}$	0.1	0.5	
Wind direction	Vane	degree	1.0	2.0	
Short-wave radiation	Pyranometer	$W\ m^{-2}$	0.1	~3%	
Long-wave radiation	Pyrgeometer	$W\ m^{-2}$	0.1	~3%	
Atmospheric temperature profile	Radiosonde	°C	0.1	0.2	
Humidity profile	Radiosonde	%	0.1	2.0	

[1] Sensors mounted on the foremast are at a height of 16 m above the water line, and those at the stern 12 m. The self-calibrating SST radiometer was mounted 8 m above the waterline.

In addition to the computer-logged measurements, the bridge officers take routine marine weather observations according to the WMO schedule, usually at 6-h intervals.

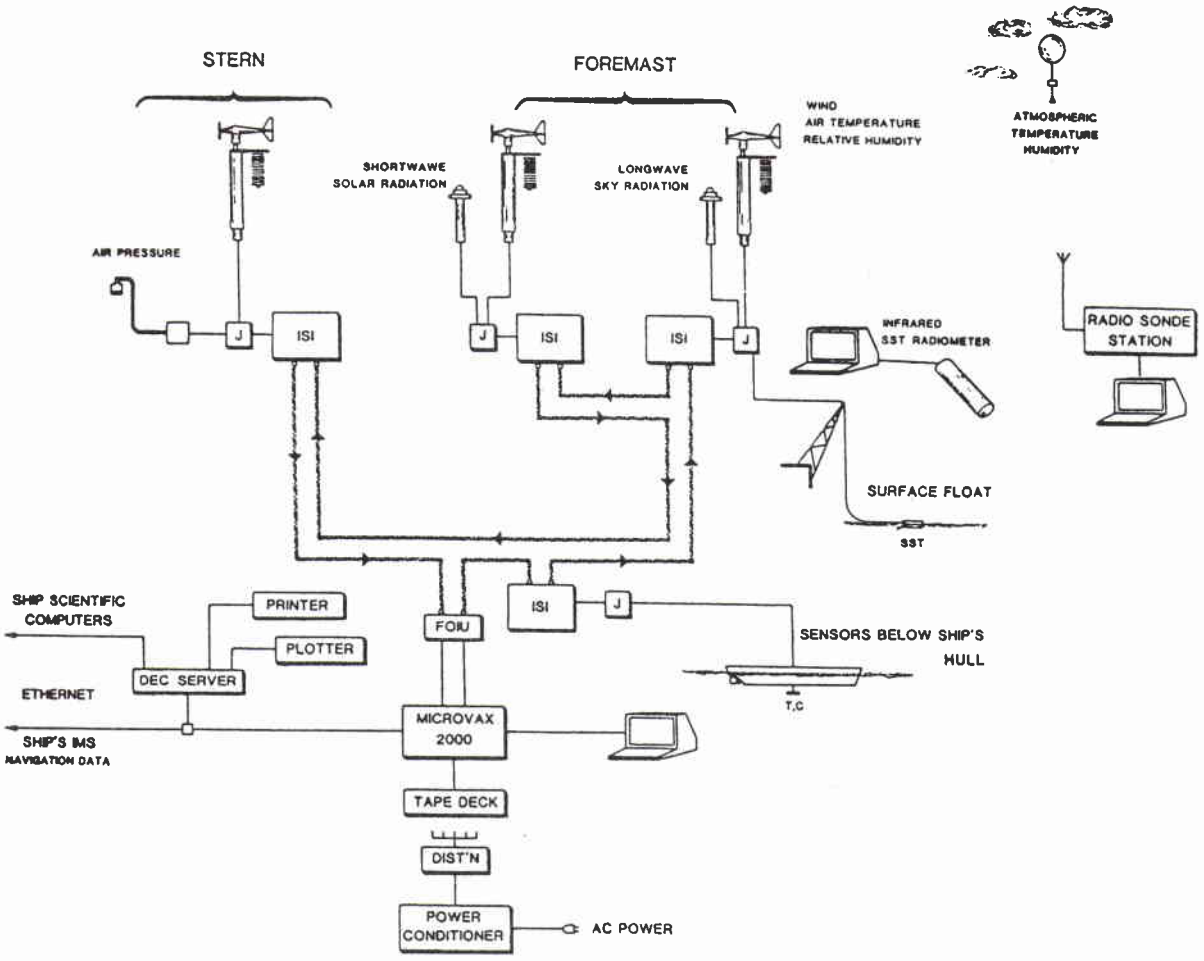

Figure 2 *Schematic representation of the instruments of the ZAN (Zeno- Alliance Network) on the RV Alliance. ISI stands for Intelligent Sensor Interface, FOIU is Fibre-Optics Interface Unit, J is Junction box, IMS is Information Management System, SST is Sea Surface Temperature, T is Temperature.*

4.2. SEA-SURFACE TEMPERATURE

Sea-surface temperature was measured by three independent instruments: an infrared radiometer detected the electromagnetic emission from the surface, a towed thermistor measured the *in situ* temperature at a notional depth of 0.1 m, and a high accuracy thermistor measured the bulk temperature at a depth of about 3 m below the water-line. The towed thermistor could only be deployed in calm to moderate seas, and when the ship's speed was below about 8 kn; as a consequence this sensor could only be occasionally used.

4.2.1. Radiometric skin temperature

The SST radiometer contains an ambient temperature detector which receives a signal from the sea-surface 'chopped' against the radiance from a black body reference target, the temperature of which is measured by a precision thermistor. At programmed intervals the instrument is internally calibrated by bringing into the field of view first a hot black-body target, and then a cold black-body target. The cold target temperature floats at ambient temperature, and is generally somewhat cooler, by 1°C, than the reference black-body. The hot black body target is heated to about 9 or 10°C above the temperature of the cold black body target. The radiometer was controlled by an IBM Personal Computer, which also logged the data onto disk. The radiometer was programmed to sample the sea-surface radiance and reference temperatures as means of generally ten or twenty independent samples, the standard deviations of which were also calculated, and to conduct a calibration cycle after about every 10 min of observations. The calibration cycle took about 2 min.

4.2.2. Bulk temperature at $\sim 0.1\ m$

The near-surface *in situ* sea-surface temperature was measured at a nominal depth of 0.1 m by a thermistor mounted in a surface-following device towed on an electromechanical cable from the forward crane, or from a boom extended sideways from the forward working-deck. This device is called the cappello and the measurements were logged by the ZAN system. The towing speed of the cappello can be limited in high sea-states, and for this reason its use was restricted during this experiment especially during transits at cruising speed.

4.2.3. Bulk temperature at $\sim 3\ m$

The bulk sea temperature was measured continually by a Sea-Bird sensor mounted on a ram that extends it through the hull at a depth of about 3 m. The sensing element is about 40 cm beyond the hull, on the forward port side about 25 m behind the bow, just forward of the level of the bridge. This is connected to the ZAN by an ISI and its sampling is not restricted by sea state nor ship's speed.

4.3. SKY RADIOMETER

A Barnes PRT-5 precision infrared radiation thermometer was mounted in the Aft Bridge, measuring through an open door, inclined skywards at about the same angle as the SST radiometer was inclined towards the sea, to measure the infrared radiation in the 9–13 μm interval arriving at the sea surface from the sky. This is a necessary correction for the radiative SST measurement, as a small fraction of the sky radiation is reflected into the SST radiometer. The sky radiation is very variable, being strongly dependent on the presence of clouds, especially low clouds with warm bases. The data were digitized and archived on an IBM Personal Computer.

Table 2a *Successful radiosonde launches (October)*

Date	Time	Position	Min. P (μPa)	Comments
02	14:46	50°19.65′N, 1°03.73′W	545	Sky clear
04	13:49	44°05.56′N, 8°40.08′W	177	Some high cloud
05	07:31	41°43.87′N, 9°26.57′W	215	Some high cirrus
05	10:39	41°00.10′N, 9°26.68′W	166	Large areas of sky clear
05	22:12	37°52.86′N, 9°18.92′W	365	Sky clear; radio noise
06	22:04	36°21.01′N, 3°30.26′W	138	Sky clear
07	08:34	37°24.91′N, 0°50.87′W	106	Sky clear, sea calm
07	14:12	38°18.90′N, 0°14.93′E	144	Perfect conditions
07	19:01	39°07.74′N, 1°13.81′E	172	Sky clear
08	08:31	41°03.21′N, 4°32.50′E	140	Very good conditions
08	13:11	41°42.57′N, 5°41.96′E	175	Very good conditions
08	18:21	42°25.80′N, 6°78.43′E	202	Very good conditions
16	18:22	44°02.76′N, 9°35.20′E	150	Very good conditions
17	08:57	44°08.44′N, 9°10.79′E	157	Some cloud, low and high
20	13:19	44°12.92′N, 9°09.94′E	265	Much cloud on horizon, atmosphere very dry
20	17:36	44°03.43′N, 9°35.18′E	328	Sky very clear, atmosphere very dry
25	06:15	42°37.24′N, 10°44.73′E	160	Sky very clear
25	10:27	42°37.43′N, 10°44.93′E	147	Sky very clear
25	13:25	42°37.40′N, 10°45.11′E	145	Sky very clear
25	18:15	42°41.21′N, 10°48.10′E	192	Sky very clear
26	07:59	42°30.56′N, 10°36.56′E	130	Sky clear, some haze
26	13:07	42°37.14′N, 10°44.91′E	130	Some high cloud, from contrails
26	18:20	42°35.49′N, 10°43.65′E	260	Sky clear
28	23:05	41°13.71′N, 8°35.54′E	193	Sky clearing after cloud
29	18:15	40°49.67′N, 7°13.82′E	251	Sky clear, after cloud
30	08:16	40°31.24′N, 6°41.13′E	130	Some cloud
30	14:08	40°36.87′N, 6°54.97′E	211	Some cloud
31	18:23	40°06.07′N, 6°12.50′E	298	Sky clear
31	23:10	40°07.35′N, 6°11.72′E	202	Sky clear

4.4. RADIOSONDES

Atmospheric profiles of temperature and humidity were made using disposable radiosondes carried aloft on helium balloons. The measurements are transmitted to a receiving station on the ship. The radiosondes were launched so their ascents coincided with satellite overpasses when the sky was reasonably clear of cloud, thereby increasing the chances of good satellite data. The radiosonde data were transferred in real time to an IBM Personal Computer for display and archiving.

Two types of radiosondes were used during the cruise, and these differed in how they measured humidity. Both types, manufactured by Atmospheric Instrument Research Inc, measured air temperature using a well exposed thermistor and barometric pressure by an aneroid barometer. For the humidity measurement, the first type used a thermistor surrounded by a wick which was kept moist by water from a small reservoir; this gives a 'wet bulb' temperature from which the humidity can be calculated by reference to the air temperature through the psychrometric rela-

Table 2b *Successful radiosonde launches (November)*

Date	Time	Position	Min. P (μPa)	Comments
01	13:17	40°26.06′N, 6°32.12′E	147	Small amount of cloud
01	14:44	40°32.40′N, 6°36.68′E	125	Small amount of cloud
01	18:39	40°48.10′N, 6°47.42′E	262	Small amount of cloud
02	09:48	40°38.73′N, 6°36.64′E	225	Sky clear
02	13:15	40°48.3 ′N, 6°50.6 ′E	125	Sky clear
02	14:42	40°48.28′N, 7°01.17′E	176	Some cloud
02	17:57	40°49.57′N, 7°11.53′E	256	Sky clear
03	19:33	42°38.48′N, 10°44.15′E	297	Some cloud
05	07:24	42°46.53′N, 10°27.01′E	460	Sky very clear
05	08:31	42°45.60′N, 10°24.76′E	260	Sky very clear
05	13:12	42°45.67′N, 10°24.69′E	423	Some cloud
05	14:18	42°43.18′N, 10°32.91′E	290	Significant cloud amount
06	06:36	42°40.25′N, 10°40.90′E	223	Significant cloud amount
07	07:57	42°38.02′N, 10°44.21′E	262	Sky very clear
07	12:49	42°38.88′N, 10°40.81′E	388	Some high cloud
07	13:40	42°38.85′N, 10°40.80′E	251	Some high cloud
07	17:44	42°36.07′N, 10°44.12′E	455	Sky clear
08	07:32	42°37.24′N, 10°45.12′E	106	Much of sky covered by thin cirrus
08	12:15	42°40.26′N, 10°41.01′E	210	Sky clear
08	13:15	42°38.34′N, 10°46.65′E	149	Sky clear
08	18:29	42°37.39′N, 10°45.07′E	259	Sky clear

tionship. In the second type relative humidity was directly measured by a carbon hygristor. The first type gives a very good humidity measurement as adequate airflow over the sensors is assured for even low ascent rates ($\sim 1\ \mathrm{m\,s^{-1}}$) by small wings that cause the sonde to rotate rapidly as it ascends. However, once the radiosonde ascends beyond the freezing level, the water over the wet thermistor freezes and the data become difficult to interpret; this is discussed further below. The second type does not suffer from this problem, but requires a more rapid ascent rate ($\sim 3\ \mathrm{m\,s^{-1}}$) to function well, thereby losing vertical resolution, and the hygristor measurement is known to loose accuracy for both very low ($< 20\%$ relative humidity) and high ($> 80\%$ relative humidity) values, and after the sensor has become physically wetted, such as may happen as the sonde ascends through cloud as well as in rain. To compare the measurements of the two types of sondes, pairs were launched on five occasions. Because they use the same radio-frequency the launches were sequential, being separated by less than one hour: the hygristor was launched first because of its more rapid ascent rate.

4.5. NAVIGATION

Navigation information are available from the ship's PLNS (Precision Location and Navigation System). The ZAN obtains values of latitude, longitude, ship's speed, heading (gyrocompass reading) and course made good, at intervals of about one minute. The PLNS synthesizes an optimum ship's navigation status from a variety of navigation aids including the Global Positioning System, Satellite Navigation and Loran-C.

4.6. INSTRUMENT PERFORMANCE

The long-wave pyrgeometer did not function during the passage from Amsterdam to La Spezia. The problem was traced to a broken cable, which was repaired on October 11 while the ship was in port. Data logging of this sensor began when the ship left port on October 16. Problems with the long-wave pyrgeometer resurfaced at the end of the cruise and measurements from the last two days (November 7 and 8) are corrupt.

Other sensors attached to the ZAN worked well. There appear to be some calibration problems with the measurements from the shipboard SST radiometer and these are not presented here. If the problems can be resolved the measurements will be the subject of a future data report.

5
Data processing

During the cruise the measurements from the ZAN were archived on disk in a FOCUS database from which derived variables and plots were generated in near real-time. Periodic inspection of the sensors took place throughout the cruise and the domes of the radiometers were cleaned at intervals of a few days. There was no evidence of dirt or salt deposition on the radiometer domes. The anemometers were inspected during and after the cruise and no evidence was found to suggest that the bearings were becoming worn thereby invalidating the calibration.

5.1. CALIBRATION

The thermometers and relative humidity sensors were calibrated before and after the cruise and these calibrations have been applied to the data presented in this report.

End-to-end calibration tests of the cappello temperature signal made during this cruise against a hand-held digital thermometer revealed a slight residual non-linearity in the thermistor response. A correction has been applied even though it only becomes significant at temperatures above ~ 18°C:

$$SST* = 1.066 * SST - 1.107, \text{for} SST > 16.6\,^{\circ}\text{C}. \tag{1}$$

Before this cruise the long-wave pyrgeometer was compared at the UK Meteorological Office with a transfer standard instrument traceable to a reference at the UK National Physical Laboratory (Grimmer, 1990), and a temperature dependence of the gain of the device was revealed to be

$$g = x * T_{\text{sink}} + y, \tag{2}$$

where T_{sink} is the instrument's sink temperature, $x = 0.1219$ and $y = 1.993$. The gain given by the manufacturer is a constant with the value 4.16 μV/(Wm^{-2}). The data were corrected using (2) with the measurement of air temperature being used as an estimate of T_{sink}. With an air temperature of 20 °C, this changes the measurement of LW$\downarrow$ by 6.6%.

Table 3 *Angles used to select the upwind wind sensors*

Upwind sensor	Relative wind direction range*
Foremast Port	205°to 15°
Foremast Starboard	15°to 145°
Stern Port	145°to 205°

* The ship's bow defines 0° relative.

5.2. DATA SELECTION

The selection of the best exposed wind sensor was made by examining the relative wind direction. The upwind sensors were selected according to the angles given in Table 3, which were determined from the measurements of an earlier cruise, and the selection of the sensors followed a similar procedure to that used on the MASTEX data (Minnett, 1992).

5.3. ICING ON THE RADIOSONDES

The freezing of the water in the wick around the wet thermistor and in the reservoir is easily identified as the latent heat of fusion causes a sudden apparent increase in the wet bulb temperature of several degrees, which persists for a minute or more, and usually causes a reversal in the sign of the wet bulb temperature depression. The sheath of ice over the wet thermistor acts to insulate the sensor from the ambient temperature (or, correctly, the temperature of the air saturated above ice), and the subsequent wet bulb temperature appears then to lag the dry bulb temperature with the result that the wet bulb temperature depression is too positive. If the time constant of the heat flow through the ice from the air to the thermistor can be determined, a simple correction can be applied to generate an estimate of the true air temperature saturated above ice, from which the humidity can be calculated.

The time constant for heat flow through the frozen wick of the wet bulb thermometer was determined for each profile by examining the recovery of the wet bulb temperature (T_w) after the increase in temperature caused by the water freezing. In an ideal situation, with the ambient conditions stationary T_w would follow an exponential curve asymptotically approaching the correct value for an aspirated psychrometric temperature over ice. In reality the ambient conditions are not stationary and the determination of the time constant of the exponential decay is subject to considerable uncertainty.

The theoretical time constant for heat flow through a 1 mm spherical sheath of ice surrounding a 1 mm radius thermistor is 1.25 s (neglecting stem conduction along the leads to the thermistor). That the empirically determined time constants are significantly longer can be explained by the larger thermal capacity of the ice volume in the reservoir which is in good thermal contact with the thermistor bead. For example, if half of the initial contents of the reservoir were to have been consumed

by the time that freezing occurs, the remaining water would have a thermal capacity of about 12 times that of a 1 mm sheath, leading to a time constant of about 16 s.

Application of a simple time constant correction improved the response of the T_w traces, (designated T'_w) so that for most of the ascents $T'_w < T_a$ (the air temperature as measured by the dry thermistor). However in nearly all cases $T'_w > T_a$ at the top of the ascent. The position at which the sign of the temperature difference changes is very variable, generally lying above 400 μPa. This is not simply a further heat flow problem that could be corrected by using a longer time constant, as T'_w does not obviously lag T_a and $T'_w - T_a$ remains quite constant as the time rates of change of the temperatures changes sign as the radiosondes pass through the tropopause and into the stratosphere, which in these data is characterized by temperatures increasing with height. The effect can not be explained by preferential solar heating of the ice-covered thermistor (the plastic reservoir protrudes slightly beyond the radiation shield) as the effect is as pronounced for ascents in darkness as for those in sunlight. The cause of this effect is as yet unresolved. A correction consisting of forcing the profile of absolute humidity to decay exponentially with pressure above a subjectively defined level was applied. The decay constant was determined by examination of the absolute humidities measured by the radiosondes equipped with carbon hygristors, as -60 μPa^{-1} for $P > 400$ μPa, and 40 μPa^{-1} for $P < 400$ μPa. To avoid unrealistically high relative humidities resulting from this correction it was necessary to reduce the decay constant to 20 μPa^{-1} for $P < 300$ μPa.

5.4. EXTENDING RADIOSONDE PROFILES TO GREAT HEIGHT

Those profiles that did not reach the tropopause were extended by merging each with the uppermost portion of the profile nearest in time that did penetrate into the stratosphere. To ensure a smooth transition an exponential weighting function was applied for a pressure interval of up to 100 μPa in extent. All profiles were extended to $P = 0.004$ μPa by appending the required portion of a standard atmosphere (Beer, 1990). This extended each profile to a height of 85 km.

5.5. GENERATION OF DERIVED VARIABLES

From the measured data it is possible to calculate a number of derived variables. These are the true wind speed, the net long-wave radiation at the sea surface and the turbulent fluxes of latent heat and sensible heat.

Although the sensors are all sampled at 1 Hz and 1 min averages are built up, the times appropriate to the average values are not exactly synchronous for all sensors. So before calculating derived variables it was necessary to resample the various time series at a common time base. For those calculations requiring the use of sea-surface temperature, all of the data streams from the individual instruments were resampled to the time base of the port foremast sensors.

The true wind speed and direction were calculated from the relative wind measurements by the removal of the ship's speed and heading, which were resampled to the times of the wind measurements.

The net long-wave radiation is the difference between the measured incoming long-wave radiation and that emitted by the sea surface at the measured sea surface temperature. A surface emissivity, ϵ, of 0.98 was used in the Stephan-Boltzmann equation:

$$LW \uparrow = \epsilon \sigma T^4, \tag{3}$$

where σ is the Stephan-Boltzmann constant ($5.67\ 10^{-8}$ $\mathrm{Wm^{-2}\ K^{-4}}$) and T is the sea-surface temperature in Kelvin. No attempt was made to model the effect of the thermal skin layer on the emitted radiation (see e.g. Robinson et al., 1984).

The net short-wave radiation at the sea-surface has been calculated by

$$SW_{\mathrm{net}} = SW \downarrow (1 - \alpha), \tag{4}$$

where $SW\downarrow$ is the measured incident short-wave radiation and α is the sea-surface albedo which for the present purposes has been taken as a constant with a value of 0.06 (Payne, 1972).

The turbulent fluxes were calculated using the standard bulk aerodynamic formulae which relate latent and sensible heat exchanges to the standard surface meteorological measurements:

$$H = \rho c_p C_H U (T - SST), \tag{5}$$

$$E = \rho L C_E U (q - q_o), \tag{6}$$

where H and E are the turbulent fluxes of sensible and latent heats to the ocean, ρ is air density, c_p is the specific heat of air, and L is the latent heat of evaporation; U, T and q are wind speed, air temperature and specific humidity measured at a given height above the sea-surface, SST is the sea-surface temperature and q_o is the specific humidity at the surface, assumed to be close to saturation (98% to allow for the effects of salinity) at the SST. The bulk transfer coefficients C_H and C_E are dependent on the sensor height on wind speed and on atmospheric stability. The coefficients used in this study were derived using the algorithms of Smith (1988) using an air temperature of 20°C and a sensor height of 16 m above the water-line, and have explicit dependence on the sensor height, wind speed and the stability of the atmospheric boundary layer.

For the purposes of this report, the turbulent fluxes, and the upwelling long-wave radiation, have been derived using the sea-temperatures measured by the Sea-Bird sensor at a depth of about 3 m. This gives better sampling and continuity than would be the case using the near-surface cappello measurements, but are less accurate when there are significant near-surface vertical temperature gradients in the water (see Appendix D).

6

Data presentation

A plot of the ship's position derived from the PLNS is shown in Fig. 1 for the whole period covered by this report. For the days during which the ship was at sea ship tracks are given in Appendix A.

Time-series plots of true wind speed and direction, air temperature, relative humidity, and surface pressure are presented in Appendix B. Each plot covers a one-day period of the cruise, and data are plotted with full temporal resolution. The spikes in the true wind direction and speed result from the imperfect compensation for the ship's motion when the vessel was making rapid manoeuvres; the relative winds being averages over one-minute intervals while the ship's navigation data are spot samples within those intervals. The large excursions in surface pressure on June 6 are associated with the erection of the stern instrument mast on which the barometer vent is mounted. Unphysical spikes in the pressure trace before this date are caused by deficient exposure of the barometer vent which was susceptible to spurious effects caused by wind.

Time series of the radiative terms of the surface heat budget are shown in Appendix C. These are the measured hemispheric downwelling short-wave radiation (insolation), and hemispheric downwelling long-wave radiation. Also shown are the calculated upwelling long-wave radiation, net long-wave radiation, and net surface radiation.

Near-surface temperature time series are given in Appendix D, with the smooth trace being the Sea-Bird measurements taken at a depth of about 3 m and resolved to 0.01°C and the discontinuous trace being the cappello measurement from about 10 cm depth and resolved to 0.1°C.

The air and sea temperatures, and their differences, are shown in Appendix E. The sea temperature is that measured at a depth of about 3 m by the Sea-Bird sensor.

The derived variables shown in Appendix F include the total turbulent air–sea heat exchange and the latent and sensible component fluxes. The Bowen ratio is the ratio between the sensible and latent heat exchanges, and the surface energy budget is the sum of the turbulent and radiative fluxes.

The atmospheric profiles are presented in Appendix G against a vertical axis of atmospheric pressure. Each profile is identified by the time and location of the radiosonde launch. The measured variables are temperature and humidity and the

absolute humidity and wet bulb depression were calculated using standard meteorological algorithms. The absolute humidity trace is shown magnified by a factor of ten as a dashed line for humidities below 1 g m^{-3}.

7 Discussion

The daily statistics of the measured and derived variables are given in Table 4, and the daily mean values of selected variables are shown in Figs. 3–6.

The winds experienced during the cruise were variable, with the strongest winds being associated with the storm in the southern North Sea at the start of the cruise, when speeds of over 20 ms^{-1} were measured. Once in the Mediterranean such speeds were measured only during one event towards the end of the cruise. The air temperatures were generally a few degrees cooler than the sea-surface temperatures, which were significantly higher in the Mediterranean than outside. The Mediterranean sea-surface temperatures decreased during the course of the cruise, as is expected given the season, but it is not clear that the rate of decrease truly reflects the autumnal cooling of the sea surface layer, or, given the extent of the cruise area, whether it included spatial changes. The surface humidity was very variable with drier atmospheric surface layers being found towards the end of the cruise.

The atmospheric profiles reveal much variability in the vertical temperature and humidity structure indicating interleaving air masses.

The measured insolation was very variable reflecting the wide range of cloud cover experienced during the cruise. The daily mean insolation was generally about half of the mean measured downwelling long-wave radiation, which in turn was smaller than the long-wave radiation emitted by the sea surface leading to a daily net long-wave radiation heat loss by the ocean often greater than 50 Wm^{-2}. These values are much lower than would be experienced in conditions of clear skies. The daily mean net surface radiation showed a gain by the ocean of less than 100 Wm^{-2}, often with mean values much smaller.

The turbulent fluxes were variable, reflecting the fluctuations in the wind, air–sea temperature differences, and surface humidity. The daily mean latent heat flux was always dominant over the sensible heat loss of the ocean, with peak daily mean turbulent heat losses sometimes in excess of 250 Wm^{-2}.

The daily mean values of the net surface energy budget were dominated by the latent heat loss and were negative, with the exception of November 2, and often greater than -150 Wm^{-2}. This heat loss to the atmosphere is to be expected given the time of year in which the measurements were made.

Table 4a *Surface heat budget statistics: Wind speed (ms^{-1}) at 16 m*

Date (Oct/ Nov)	N[1]	Mean	Stand. dev.	Min.	Max.
1*	270	17.228	2.216	11.760	22.400
2	1043	9.736	3.843	4.480	22.980
3	710	7.616	0.780	4.750	10.080
4	720	7.352	1.919	2.030	12.190
5	720	10.287	2.474	5.060	21.040
6	720	6.907	2.717	1.670	14.270
7	720	4.111	2.043	0.580	9.510
8	720	2.878	1.884	0.050	7.180
9*	200	4.534	1.082	2.320	7.250
16*	417	2.466	1.140	0.210	5.560
17*	568	7.720	2.596	2.440	14.430
19*	305	7.125	2.672	1.410	13.690
20*	559	5.885	2.862	0.380	13.800
24*	92	3.781	1.281	1.660	7.240
25	720	3.269	1.927	0.130	7.460
26	720	5.571	2.250	0.650	11.140
27	700	8.895	1.090	2.140	11.390
28	720	8.313	3.293	1.170	15.180
29	710	6.877	1.880	1.510	12.740
30	720	4.919	2.123	0.350	9.370
31	719	6.508	1.636	1.020	10.050
1	662	6.043	2.030	1.700	10.280
2	695	4.016	2.074	0.100	11.670
3	616	6.318	2.812	1.700	15.530
4	713	11.891	2.942	1.030	17.570
5	714	9.655	4.088	0.460	20.730
6	718	7.561	2.272	1.450	13.400
7	720	8.064	2.171	4.520	14.600
8*	503	4.997	1.606	0.280	9.640

[1] N is the number of 1-min averages used to compute the statistics.
* Days for which the statistics are calculated for a period of less than 24 h.

Table 4b *Surface heat budget statistics: Air pressure (μPa)*

Date (Oct/ Nov)	N[1]	Mean	Stand. dev.	Min.	Max.
1*	110	1005.890	1.529	1003.780	1009.530
2	811	1025.704	3.924	1009.349	1027.890
3	711	1027.081	1.426	1024.329	1029.079
4	721	1023.075	2.753	1018.650	1028.250
5	721	1020.485	0.981	1018.150	1022.119
6	721	1015.531	0.944	1013.090	1018.229
7	721	1013.389	1.778	1010.809	1015.940
8	721	1010.425	0.988	1009.059	1013.059
9*	201	1013.737	0.964	1012.750	1016.179
16*	418	1017.593	0.604	1016.409	1018.400
17*	573	1015.365	1.273	1011.809	1017.450
19*	479	1003.509	1.643	1001.099	1007.059
20*	559	1007.639	2.472	1003.090	1012.289
24*	95	1021.901	0.175	1021.659	1022.309
25	721	1019.707	1.032	1018.309	1021.669
26	721	1018.050	0.554	1017.280	1019.030
27	701	1016.572	0.606	1015.380	1017.679
28	721	1015.044	1.144	1013.059	1017.369
29	711	1017.909	0.502	1016.849	1018.900
30	721	1018.987	0.468	1017.690	1019.830
31	721	1016.707	1.471	1014.369	1019.940
1	665	1022.271	1.573	1019.880	1024.530
2	707	1023.482	0.983	1020.979	1025.069
3	626	1016.012	2.398	1012.250	1020.989
4	720	1004.298	3.528	1000.130	1012.309
5	720	1005.603	2.634	1001.530	1010.320
6	718	1012.547	2.908	1009.059	1018.840
7	720	1021.726	1.414	1018.780	1023.960
8*	549	1019.061	1.851	1015.289	1021.780

[1] N is the number of 1-min averages used to compute the statistics.
* Days for which the statistics are calculated for a period of less than 24 h.

Table 4c *Surface heat budget statistics: Air temperature (° C)*

Date (Oct/ Nov)	N[1]	Mean	Stand. dev.	Min.	Max.
1*	272	15.791	0.726	14.000	16.600
2	1044	15.019	1.296	11.800	16.400
3	710	15.725	0.617	14.900	17.200
4	720	17.587	0.703	16.100	18.600
5	720	17.807	1.018	16.100	19.799
6	720	20.365	1.260	17.200	22.200
7	720	20.622	0.920	19.000	22.400
8	720	20.150	0.497	19.200	21.400
9	200	19.188	0.916	15.600	19.900
16*	417	19.573	0.367	18.799	21.000
17*	572	19.911	0.323	19.299	21.000
19*	478	17.825	0.703	15.200	18.799
20*	559	15.648	1.087	13.900	17.799
24*	94	14.176	1.162	11.800	15.700
25	720	16.004	1.267	13.600	18.400
26	720	16.267	1.389	13.400	18.299
27	700	16.014	0.944	14.400	17.299
28	720	17.535	0.993	15.400	19.799
29	710	17.414	0.365	16.299	18.000
30	720	17.883	0.176	17.500	18.600
31	719	18.094	0.604	16.600	19.200
1	663	18.307	0.774	16.900	19.400
2	1259	19.348	0.239	18.000	20.000
3	622	18.796	0.539	17.299	19.600
4	718	19.765	0.471	18.799	20.700
5	720	17.615	0.491	15.700	18.900
6	719	14.273	1.303	12.500	17.500
7	720	14.545	0.887	13.000	15.900
8*	1085	15.011	0.920	13.400	16.799

[1] N is the number of 1-min averages used to compute the statistics.
* Days for which the statistics are calculated for a period of less than 24 h.

Table 4d *Surface heat budget statistics: Sea-surface temperature at 3 m depth (° C)*

Date (Oct/ Nov)	N[1]	Mean	Stand. dev.	Min.	Max.
1*	543	17.099	0.128	16.930	17.330
2	1421	16.864	0.275	16.110	17.240
3	1414	16.057	0.748	14.790	17.320
4	1440	17.517	0.343	16.160	18.030
5	1439	17.181	0.732	15.450	18.170
6	1439	19.638	1.101	17.270	20.860
7	1439	21.266	1.391	19.580	23.490
8	1437	21.865	1.004	20.440	23.469
9*	401	21.323	0.104	21.180	21.540
16*	824	21.326	0.201	20.830	21.629
17*	1132	21.591	0.100	21.180	21.709
19*	954	20.561	0.307	20.080	21.040
20*	1111	20.921	0.156	20.090	21.059
24*	186	18.903	0.105	18.760	19.080
25	1437	20.243	0.376	18.990	20.580
26	1440	20.388	0.047	20.280	20.490
27	1439	20.271	0.038	20.180	20.330
28	1435	19.935	0.317	18.980	20.230
29	1418	20.003	0.138	19.730	20.260
30	1440	19.705	0.196	19.100	19.889
31	1439	19.341	0.394	18.760	20.030
1	1369	19.797	0.203	19.410	20.010
2	1408	19.566	0.145	19.299	19.830
3	1240	19.509	0.317	18.600	19.770
4	1431	19.671	0.048	19.570	19.760
5	1432	19.565	0.092	19.420	19.709
6	1430	19.421	0.102	19.190	19.620
7	1434	19.206	0.064	18.990	19.299
8*	1092	19.031	0.090	18.870	19.200

[1] N is the number of 1-min averages used to compute the statistics.
* Days for which the statistics are calculated for a period of less than 24 h.

Table 4e *Surface heat budget statistics: Air–sea temperature difference (° C)*

Date (Oct/ Nov)	N^1	Mean	Stand. dev.	Min.	Max.
1*	272	−1.188	0.760	−3.080	−0.350
2	1044	−1.984	1.414	−5.410	−0.480
3	710	0.282	0.885	−0.840	2.280
4	720	−0.044	0.517	−1.170	0.930
5	720	1.025	0.591	−0.200	2.550
6	720	1.388	1.511	−1.070	3.990
7	720	0.678	0.824	−0.730	2.600
8	720	−2.645	0.373	−3.430	−1.810
9*	200	−2.048	0.913	−5.700	−1.350
16*	417	−1.647	0.372	−2.410	−0.210
17*	572	−1.687	0.330	−2.310	−0.600
19*	478	−2.514	0.661	−4.910	−1.470
20*	559	−5.266	1.083	−6.930	−3.120
24*	94	−4.730	1.096	−7.020	−3.320
25	720	−4.007	1.103	−6.190	−1.850
26	720	−4.120	1.417	−7.030	−2.020
27	700	−4.254	0.953	−5.870	−3.020
28	720	−2.603	0.987	−4.730	−0.330
29	710	−2.501	0.413	−3.710	−1.850
30	720	−1.863	0.238	−2.360	−1.200
31	719	−0.920	0.667	−2.440	0.380
1	663	−1.665	0.779	−3.110	−0.560
2	1259	−0.205	0.292	−1.530	0.530
3	622	−0.511	0.411	−1.640	0.300
4	718	0.100	0.505	−0.930	1.080
5	720	−1.929	0.451	−3.740	−0.790
6	719	−5.200	1.306	−7.040	−2.070
7	720	−4.636	0.942	−6.230	−3.230
8*	1085	−4.020	0.982	−5.740	−2.080

[1] N is the number of 1-min averages used to compute the statistics.
* Days for which the statistics are calculated for a period of less than 24 h.

Table 4f *Surface heat budget statistics: Relative humidity (%)*

Date (Oct/ Nov)	N^1	Mean	Stand. dev.	Min.	Max.
1*	272	64.535	3.723	56.500	74.699
2	1044	79.707	6.777	62.799	94.500
3	710	100.246	2.342	93.400	104.199
4	720	90.556	6.407	79.000	102.400
5	720	85.513	5.054	76.599	94.199
6	720	91.038	4.682	79.400	100.699
7	720	84.377	3.971	77.300	94.400
8	720	71.058	5.498	60.200	80.699
9*	200	76.704	4.374	66.599	85.599
16*	417	78.778	3.940	65.099	85.199
17*	572	75.016	3.274	66.400	82.900
19*	478	58.180	9.009	35.900	71.000
20*	559	43.484	7.894	29.900	61.400
24*	94	77.645	6.350	61.200	86.300
25	720	72.292	7.062	59.099	84.599
26	720	69.246	9.031	55.200	83.599
27	700	75.255	2.515	68.699	82.099
28	720	85.162	5.093	73.800	94.699
29	710	76.527	3.331	69.000	85.900
30	720	72.769	2.412	65.300	79.900
31	719	80.747	6.133	70.199	95.099
1	663	80.511	4.745	69.400	87.199
2	695	84.582	2.311	78.200	90.700
3	622	88.523	3.513	78.099	96.500
4	718	82.002	11.907	41.700	91.500
5	720	54.758	8.462	29.200	72.900
6	719	68.990	6.887	48.900	81.300
7	720	57.248	8.230	41.200	73.099
8*	1085	79.172	7.312	54.299	87.199

[1] N is the number of 1-min averages used to compute the statistics.
* Days for which the statistics are calculated for a period of less than 24 h.

Table 4g *Surface heat budget statistics: Specific humidity at sea surface (g kg^{-1})*

Date (Oct/ Nov)	N^1	Mean	Stand. dev.	Min.	Max.
1*	270	11.903	0.081	11.798	12.027
2	1043	11.473	0.247	10.954	11.946
3	710	10.915	0.510	10.063	11.801
4	720	12.020	0.256	11.037	12.393
5	720	11.805	0.544	10.543	12.586
6	720	13.870	0.932	11.919	14.920
7	720	15.404	1.359	13.804	17.640
8	720	16.005	0.999	14.645	17.624
9*	200	15.399	0.085	15.273	15.579
16*	417	15.346	0.186	14.881	15.623
17*	568	15.632	0.095	15.273	15.780
19*	305	14.941	0.292	14.440	15.285
20*	559	15.112	0.154	14.284	15.283
24*	94	13.134	0.087	13.014	13.281
25	720	14.319	0.340	13.209	14.635
26	720	14.469	0.044	14.367	14.556
27	700	14.385	0.035	14.305	14.443
28	720	14.110	0.284	13.273	14.380
29	710	14.128	0.121	13.893	14.364
30	720	13.853	0.166	13.353	14.009
31	719	13.573	0.319	13.095	14.120
1	662	13.882	0.194	13.524	14.106
2	695	13.672	0.134	13.463	13.910
3	616	13.729	0.287	12.929	13.983
4	713	14.027	0.063	13.896	14.124
5	714	13.914	0.081	13.795	14.089
6	719	13.696	0.118	13.454	13.903
7	720	13.389	0.061	13.209	13.499
8*	505	13.273	0.114	11.532	13.436

[1] N is the number of 1-min averages used to compute the statistics.
* Days for which the statistics are calculated for a period of less than 24 h.

Table 4h *Surface heat budget statistics: Specific humidity at 16 m height (g kg^{-1})*

Date (Oct/ Nov)	N[1]	Mean	Stand. dev.	Min.	Max.
1*	270	7.199	0.273	6.407	8.120
2	1043	8.367	1.201	6.358	10.288
3	710	10.923	0.454	10.103	11.927
4	720	11.133	0.378	10.129	12.134
5	720	10.694	0.379	9.884	11.566
6	720	13.501	1.323	10.577	15.342
7	720	12.698	0.617	11.227	13.989
8	720	10.433	1.037	8.736	12.778
9*	200	10.543	0.482	9.293	11.278
16*	417	11.054	0.449	9.262	11.694
17*	568	10.771	0.389	9.603	11.799
19*	305	7.002	1.295	4.749	9.073
20*	559	4.761	0.613	3.634	6.339
24*	94	7.669	0.400	6.647	8.236
25	720	8.048	0.489	6.678	9.307
26	720	8.754	0.461	7.415	9.757
27	700	8.437	0.349	7.626	9.371
28	720	10.541	0.699	8.896	11.895
29	710	9.367	0.320	8.448	10.382
30	720	9.169	0.275	8.180	10.017
31	719	10.331	0.698	8.403	11.562
1	662	10.425	1.030	8.259	11.781
2	695	11.614	0.236	11.074	12.312
3	616	11.858	0.525	10.306	12.706
4	713	11.848	1.751	6.103	13.690
5	714	6.867	1.078	3.875	9.051
6	719	6.933	0.676	4.863	8.649
7	720	5.772	0.549	4.357	7.167
8*	505	7.887	0.900	5.709	9.072

[1] N is the number of 1-min averages used to compute the statistics.
* Days for which the statistics are calculated for a period of less than 24 h.

Table 4i *Surface heat budget statistics: Net insolation (Wm^{-2})*

Date (Oct/ Nov)	N[1]	Mean	Stand. dev.	Min.	Max.
1*	268	19.653	45.244	0.190	314.149
2	1043	136.683	187.198	0.000	553.000
3	710	53.001	74.434	0.000	308.700
4	720	136.510	202.499	0.000	633.369
5	720	190.315	244.254	0.000	651.510
6	720	192.776	260.519	0.470	707.070
7	720	184.883	239.850	2.070	641.640
8	720	172.686	224.943	1.600	609.210
9*	200	14.341	29.833	1.600	127.650
16*	417	.583	192.620	1.880	680.650
17*	568	142.099	182.096	2.070	678.020
19*	305	14.306	28.258	0.000	108.480
20*	559	140.890	180.751	0.000	687.520
24*	83	0.174	0.214	0.000	0.660
25	720	143.660	200.195	0.000	540.219
26	720	134.394	189.795	0.000	522.450
27	700	40.038	61.841	0.000	315.089
28	720	74.120	120.352	0.000	616.359
29	710	51.143	95.757	0.000	685.169
30	720	119.153	174.388	0.000	573.020
31	719	52.591	79.133	0.000	319.130
1	662	97.799	164.321	0.000	543.039
2	695	127.801	186.990	0.470	642.580
3	616	31.633	52.326	0.000	389.350
4	713	36.436	57.833	0.000	307.760
5	714	120.662	181.628	0.000	530.539
6	719	39.038	87.875	0.000	513.239
7	720	117.924	175.848	0.000	503.559
8*	505	160.507	175.550	0.000	484.850

[1] N is the number of 1-min averages used to compute the statistics.
* Days for which the statistics are calculated for a period of less than 24 h.

Table 4j *Surface heat budget statistics: Downwelling long-wave radiation (Wm^{-2})*

Date (Oct/ Nov)	N[1]	Mean	Stand. dev.	Min.	Max.
16*	417	342.476	17.436	321.059	392.869
17*	568	356.412	21.461	322.119	392.670
19*	305	358.479	22.923	312.980	399.609
20*	559	361.389	34.025	304.579	408.170
24*	94	339.150	12.800	324.239	366.230
25	720	334.231	17.058	307.000	408.010
26	720	363.621	30.078	310.750	420.429
27	700	409.057	15.745	370.290	445.589
28	720	394.114	15.833	343.260	430.359
29	710	378.477	24.827	332.470	427.920
30	720	374.888	18.508	335.829	419.179
31	719	389.625	18.572	345.130	422.679
1*	662	356.807	12.736	329.489	418.290
2	695	367.851	18.856	329.260	400.070
3	616	395.969	13.218	342.299	424.119
4	713	368.841	24.956	295.299	402.649
5	714	347.631	27.827	301.100	416.679
6	719	428.546	38.452	343.609	556.140

[1] N is the number of 1-min averages used to compute the statistics.
* Days for which the statistics are calculated for a period of less than 24 h.

Table 4k *Surface heat budget statistics: Emitted long-wave radiation (Wm^{-2})*

Date (Oct/ Nov)	N[1]	Mean	Stand. dev.	Min.	Max.
1*	270	394.409	0.696	393.500	395.399
2	1043	392.828	1.552	389.070	395.130
3	710	388.809	4.021	382.010	395.619
4	720	396.692	1.871	389.329	399.500
5	720	394.876	3.972	385.529	400.269
6	720	408.429	6.119	395.339	415.200
7	720	417.615	7.908	408.070	430.320
8	720	421.006	5.738	412.950	430.200
9*	200	417.877	0.593	417.070	419.109
16*	417	417.908	1.145	415.140	419.619
17*	568	419.408	0.564	417.119	420.079
19*	305	414.092	1.832	410.920	416.269
20*	559	415.602	0.883	410.920	416.269
24*	94	404.310	0.584	403.519	405.290
25	720	411.786	2.106	404.790	413.679
26	720	412.601	0.268	412.049	413.170
27	700	411.942	0.218	411.429	412.269
28	720	410.061	1.772	404.739	411.709
29	710	410.437	0.772	408.910	411.880
30	720	408.775	1.097	405.399	409.799
31	719	406.745	2.195	403.519	410.529
1	662	409.247	1.132	407.130	410.480
2	695	408.001	0.818	406.619	409.470
3	616	407.690	1.742	402.640	409.130
4	713	408.580	0.270	408.019	409.079
5	714	407.984	0.513	407.239	408.799
6	719	407.189	0.568	406.010	408.299
7	720	405.993	0.357	404.790	406.459
8*	505	405.014	0.748	392.679	405.899

[1] N is the number of 1-min averages used to compute the statistics.
* Days for which the statistics are calculated for a period of less than 24 h.

Table 41 *Surface heat budget statistics: Net long-wave radiation (Wm^{-2})*

Date (Oct/ Nov)	N[1]	Mean	Stand. dev.	Min.	Max.
16*	417	−75.431	17.595	−98.339	−26.580
17*	568	−62.995	21.570	−97.389	−25.690
19*	305	−55.613	24.552	−102.669	−11.430
20*	559	−54.213	34.064	−111.690	−7.480
24*	94	−65.159	13.148	−80.550	−37.619
25	720	−77.555	17.237	−106.230	−4.490
26	720	−48.980	30.102	−102.139	8.160
27	700	−2.885	15.717	−41.700	33.709
28	720	−15.946	15.858	−68.389	19.379
29	710	−31.960	24.849	−78.849	17.950
30	720	−33.887	18.790	−73.529	10.160
31	719	−17.119	19.858	−65.400	17.549
1	662	−52.440	12.294	−78.419	7.930
2	695	−40.149	18.798	−79.150	−8.680
3	616	−11.720	13.932	−66.160	17.110
4	713	−39.738	24.988	−113.500	−5.810
5	714	−60.352	27.514	−106.250	8.440
6	719	21.356	38.463	−64.690	148.460

[1] N is the number of 1-min averages used to compute the statistics.
* Days for which the statistics are calculated for a period of less than 24 h.

Table 4m *Surface heat budget statistics: Net surface radiation (Wm^{-2})*

Date (Oct/ Nov)	N^1	Mean	Stand. dev.	Min.	Max.
16*	417	63.152	199.585	−95.330	635.299
17*	568	79.104	183.562	−95.320	627.570
19*	305	−41.306	45.640	−101.730	78.180
20*	559	86.676	177.253	−103.989	640.010
24*	94	−65.095	13.023	−80.550	−36.959
25	720	66.105	211.128	−105.760	531.869
26	720	85.413	185.310	−100.730	465.079
27	700	37.137	65.656	−41.040	307.790
28	720	58.164	118.831	−59.980	600.020
29	710	19.183	110.506	−78.379	692.599
30	720	85.266	176.959	−68.410	562.270
31	719	35.471	88.22	−65.400	316.470
1	662	45.359	167.841	−77.940	497.700
2	695	87.652	194.458	−75.669	633.900
3	616	19.913	55.448	−64.750	383.420
4	713	−3.302	65.036	−111.430	276.480
5	714	60.309	167.865	−92.019	443.809
6	719	60.375	94.158	−64.500	529.710

[1] N is the number of 1-min averages used to compute the statistics.
* Days for which the statistics are calculated for a period of less than 24 h.

Table 4n *Surface heat budget statistics: Net surface radiation ($Wm^{-}2$)*

Date (Oct/ Nov)	N[1]	Mean	Stand. dev.	Min.	Max.
16*	417	−10.262	200.463	−626.429	174.899
17*	568	66.424	179.330	−482.390	271.850
19*	305	281.103	146.677	10.200	582.989
20*	559	196.010	249.875	−499.470	564.130
24*	94	184.942	35.533	−3.950	262.010
25	720	49.911	222.515	−448.890	315.730
26	720	76.689	217.452	−366.649	333.399
27	700	204.039	79.868	−42.939	321.010
28	720	80.232	167.748	−509.540	318.149
29	710	123.802	121.055	−574.729	265.519
30	720	14.102	186.934	−496.839	230.539
31	719	49.973	114.063	−272.049	261.269
1	662	44.914	161.247	−386.470	271.989
2	695	−59.155	194.764	−609.919	138.279
3	616	25.441	59.725	−326.779	141.809
4	713	85.323	122.796	−230.529	447.489
5	714	191.829	169.899	−271.959	562.950
6	719	185.137	124.027	−368.059	383.070

[1] N is the number of 1-min averages used to compute the statistics.
* Days for which the statistics are calculated for a period of less than 24 h.

Table 4o *Surface heat budget statistics: Latent heat flux (Wm^{-2})*

Date (Oct/ Nov)	N[1]	Mean	Stand. dev.	Min.	Max.
1*	270	267.267	44.098	165.595	376.799
2	1043	114.341	84.226	16.756	385.949
3	710	0.228	18.617	−38.478	25.778
4	720	20.998	12.507	−5.187	54.906
5	720	39.127	25.819	−1.362	131.643
6	720	10.312	17.010	−26.139	76.794
7	720	36.215	20.110	6.662	101.048
8	720	59.565	23.966	2.400	105.399
9*	200	85.570	19.119	49.785	152.571
16*	417	46.077	17.023	6.581	82.901
17*	568	130.274	35.608	46.469	240.954
19*	305	212.559	94.236	70.717	424.656
20*	559	238.331	84.148	30.116	441.214
24*	94	91.798	27.160	−32.128	153.906
25	720	91.878	43.016	5.834	182.877
26	720	128.088	46.876	22.636	231.185
27	700	193.189	27.554	65.271	261.434
28	720	110.974	60.091	14.446	264.440
29	710	120.343	25.560	42.019	205.549
30	720	87.302	29.190	10.917	144.936
31	719	74.796	31.345	12.016	169.402
1	662	78.141	37.810	14.487	174.926
2	695	27.307	12.000	0.903	79.439
3	616	40.373	16.711	13.346	91.015
4	713	83.343	75.906	0.263	370.488
5	714	230.609	84.987	22.172	470.000
6	719	193.640	48.303	63.535	304.408
7	720	230.079	42.722	152.347	389.259
8*	505	107.607	23.877	11.321	190.949

[1] N is the number of 1-min averages used to compute the statistics.
* Days for which the statistics are calculated for a period of less than 24 h.

Table 4p *Surface heat budget statistics: Sensible heat flux (Wm^{-2})*

Date (Oct/ Nov)	N[1]	Mean	Stand. dev.	Min.	Max.
1*	270	26.385	19.061	6.164	73.986
2	1043	24.620	26.344	1.008	93.313
3	710	3.212	9.503	−17.417	18.102
4	720	−0.284	5.492	−9.169	12.873
5	720	−6.539	6.546	−20.504	15.047
6	720	−3.826	4.196	−17.786	10.399
7	720	2.757	3.026	−4.516	9.748
8	720	5.374	2.278	0.358	11.225
9*	200	13.757	8.923	4.663	43.946
16*	417	6.811	3.482	0.155	17.072
17*	568	15.254	4.325	4.757	28.154
19*	305	27.237	17.498	8.636	79.300
20*	559	44.354	22.191	3.229	100.713
24*	94	28.047	−13.544	12.855	58.720
25	720	24.137	17.105	0.825	63.306
26	720	34.014	19.177	3.192	72.701
27	700	47.987	14.208	13.903	79.691
28	720	27.422	20.653	1.025	82.035
29	710	22.642	6.769	9.442	51.618
30	720	12.066	5.688	1.449	24.731
31	719	10.649	7.379	0.106	31.131
1	662	12.132	7.883	0.147	31.426
2	695	1.189	2.379	−2.782	13.680
3	616	4.980	3.129	0.029	15.627
4	713	−1.322	−5.752	15.870	9.650
5	714	21.529	8.295	2.055	49.141
6	719	51.900	21.342	10.762	100.649
7	720	49.928	18.694	22.640	93.427
8*	505	23.221	5.993	2.557	45.327

[1] N is the number of 1-min averages used to compute the statistics.
* Days for which the statistics are calculated for a period of less than 24 h.

Table 4q *Surface heat budget statistics: Turbulent heat flux (Wm^{-2})*

Date (Oct/ Nov)	N[1]	Mean	Stand. dev.	Min.	Max.
1*	270	293.652	58.980	175.234	450.785
2	1043	138.962	109.754	19.808	458.681
3	710	3.441	27.729	−55.896	43.881
4	720	20.714	11.303	−14.356	51.514
5	720	32.588	27.711	−8.893	145.596
6	720	6.486	19.046	−36.034	86.805
7	720	38.972	22.703	4.242	110.728
8	720	64.939	25.249	2.759	116.624
9*	200	99.327	27.742	54.449	195.205
16*	417	52.889	20.206	7.612	99.974
17*	568	145.528	38.762	51.227	255.715
19*	305	239.796	108.673	79.353	503.956
20*	559	282.686	105.032	33.346	533.955
24*	94	119.845	39.944	−44.984	212.626
25	720	116.016	59.798	6.659	246.184
26	720	162.102	65.390	25.828	300.834
27	700	241.177	40.903	79.174	341.126
28	720	138.397	79.019	15.472	317.421
29	710	142.986	31.365	51.671	253.746
30	720	99.369	34.686	12.367	166.796
31	719	85.445	37.320	12.271	200.534
1	662	90.274	45.502	14.634	206.034
2	695	28.497	13.428	0.969	93.119
3	616	45.354	17.721	13.849	93.881
4	713	82.021	76.936	−0.768	0.102
5	714	252.138	91.376	24.227	516.106
6	719	245.513	67.820	80.067	401.755
7	720	280.008	58.831	181.587	479.779
8*	505	130.848	28.474	13.878	225.888

[1] N is the number of 1-min averages used to compute the statistics.
* Days for which the statistics are calculated for a period of less than 24 h.

Table 4r *Surface heat budget statistics: Bowen ratio*

Date (Oct/ Nov)	N[1]	Mean	Stand. dev.	Min.	Max.
1*	270	0.093	0.057	0.032	0.242
2	1043	0.167	0.085	0.022	0.366
3	710	−0.126	9.285	−219.541	8.595
4	720	0.363	10.630	−43.585	271.777
5	720	5.013	120.931	−14.390	3170.826
6	720	−0.413	3.572	−58.371	50.027
7	720	0.058	0.077	−0.363	0.157
8	720	0.102	0.042	0.014	0.178
9*	200	0.149	0.057	0.087	0.326
16*	417	0.141	0.037	0.017	0.213
17*	568	0.120	0.026	0.039	0.161
19*	305	0.126	0.035	0.068	0.215
20*	559	0.176	0.042	0.098	0.249
24*	94	0.297	0.067	0.172	0.410
25	720	0.233	0.068	0.111	0.358
26	720	0.245	0.070	0.133	0.364
27	700	0.244	0.042	0.185	0.315
28	720	0.228	0.075	0.048	0.384
29	710	0.187	0.033	0.134	0.280
30	720	0.133	0.022	0.085	0.179
31	719	0.135	0.077	0.002	0.365
1	662	0.133	0.054	0.008	0.198
2	695	0.042	0.058	−0.105	0.191
3	616	0.132	0.082	0.001	0.370
4	713	−0.071	0.176	−0.768	0.102
5	714	0.097	0.026	0.032	0.214
6	719	0.261	0.060	0.094	0.351
7	720	0.212	0.052	0.135	0.299
8*	505	0.218	0.038	0.165	0.334

[1] N is the number of 1-min averages used to compute the statistics.
* Days for which the statistics are calculated for a period of less than 24 h.

Table 4s *Surface heat budget statistics: Surface energy flux (Wm^{-2})*

Date (Oct/ Nov)	N[1]	Mean	Stand. dev.	Min.	Max.
16*	417	−10.262	200.463	−626.429	174.899
17*	568	66.424	179.330	−482.390	271.850
19*	305	281.103	146.677	10.200	582.989
20*	559	196.010	249.875	−499.470	564.130
24*	94	184.942	35.533	−3.950	262.010
25	720	49.911	222.515	−448.890	315.730
26	720	76.689	217.452	−366.649	333.399
27	700	204.039	79.868	−42.939	321.010
28	720	80.232	167.748	−509.540	318.149
29	710	123.802	121.055	−574.729	265.519
30	720	14.102	186.934	−496.839	230.539
31	719	49.973	114.063	−272.049	261.269
1*	662	44.914	161.247	−386.470	271.989
2	695	−59.155	194.764	−609.919	138.279
3	616	25.441	59.725	−326.779	141.809
4	713	85.323	122.796	−230.529	447.489
5	714	191.829	169.899	−271.959	562.950
6	719	185.137	124.027	−368.059	383.070

[1] N is the number of 1-min averages used to compute the statistics.
* Days for which the statistics are calculated for a period of less than 24 h.

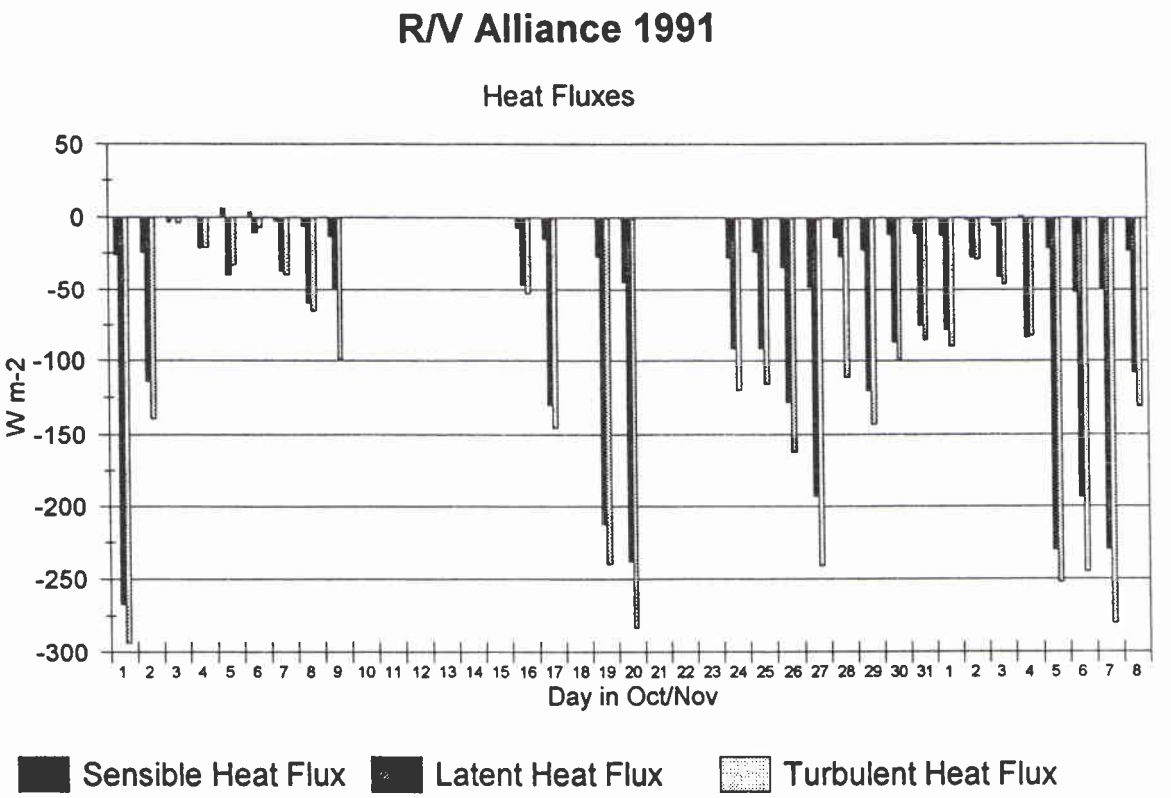

Figure 3 *Bar chart of the daily mean components and resultant measured turbulent air–sea heat fluxes. Negative values indicate heat loss by the ocean.*

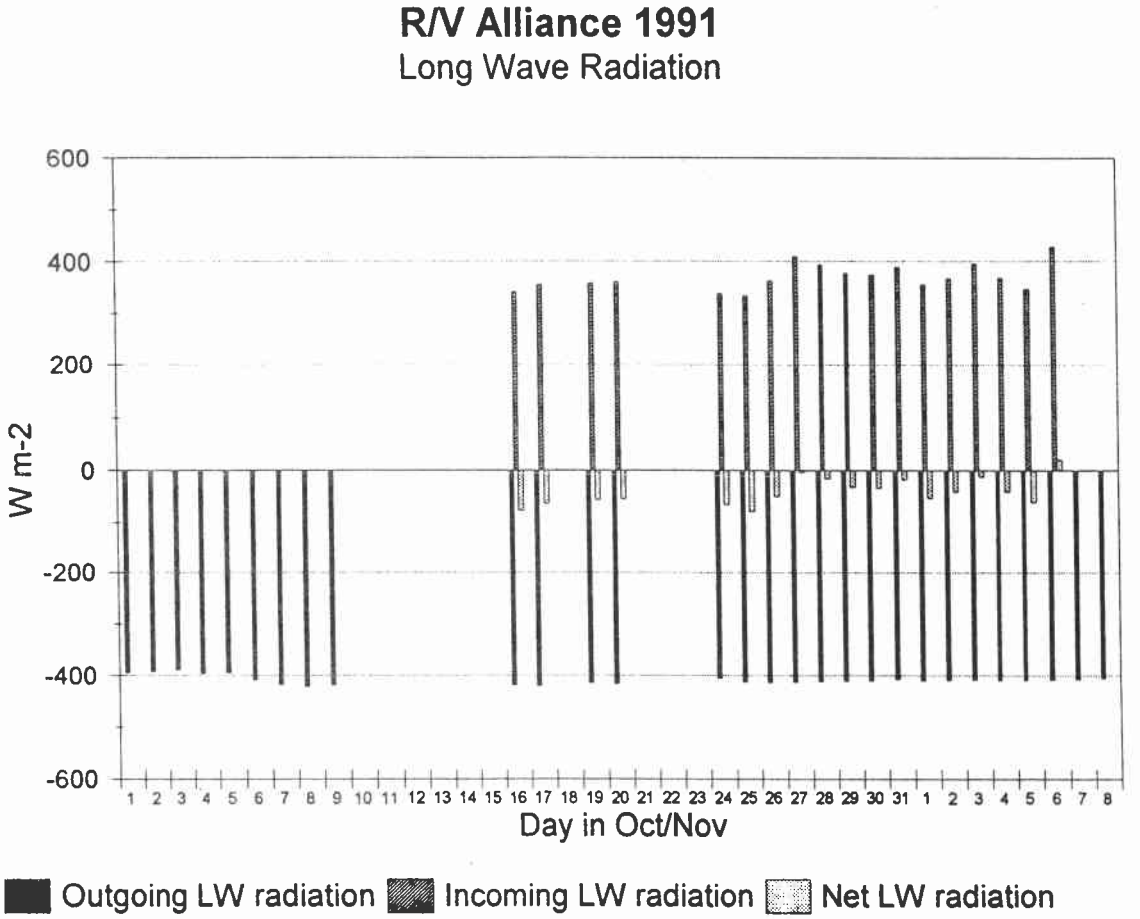

Figure 4 *Bar chart of the daily mean values of the measured incoming hemispheric long-wave radiation, calculated emitted long-wave radiation, and resultant, at the ocean surface. Negative values indicate heat loss by the ocean.*

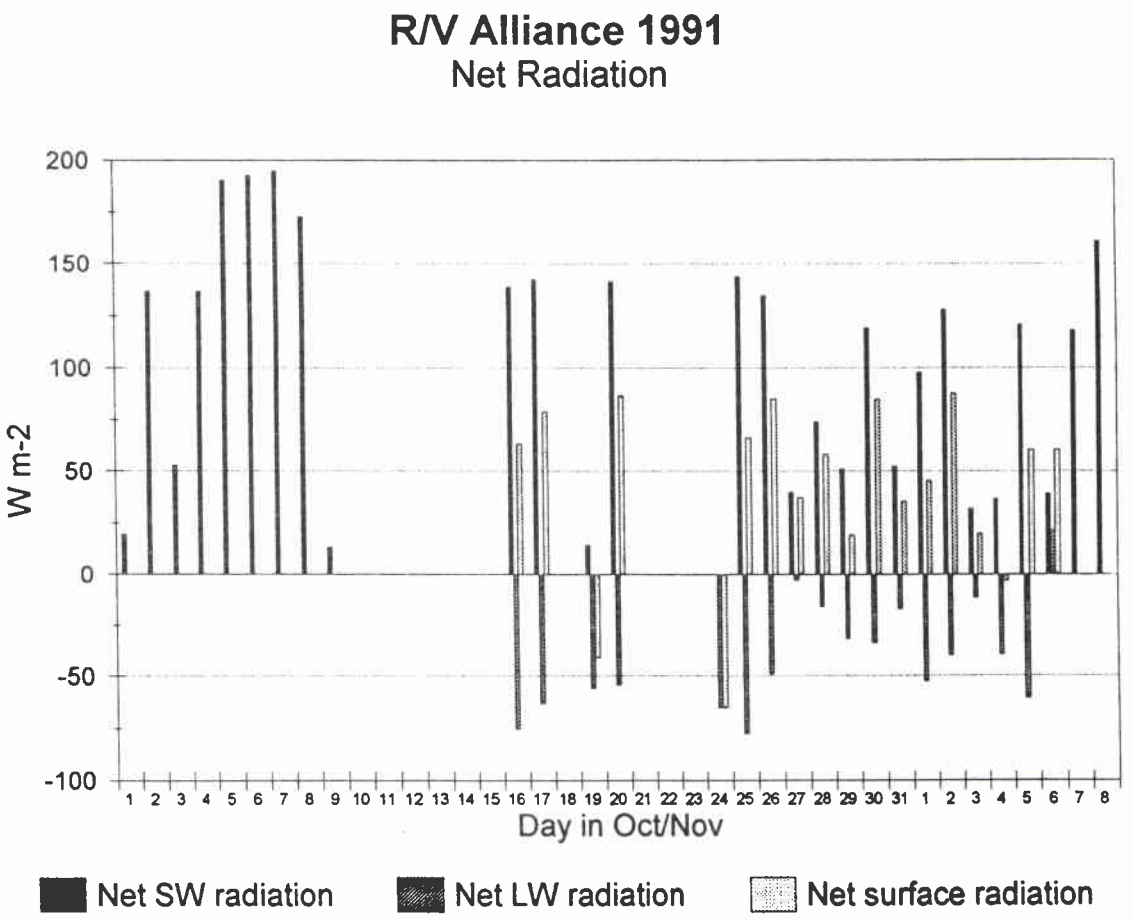

Figure 5 *Bar chart of the daily mean net short-wave and long-wave radiation and resultant surface radiation budget. The measured insolation can be recovered from the net short-wave values by multiplication by 1/0.94. Negative values indicate heat loss by the ocean.*

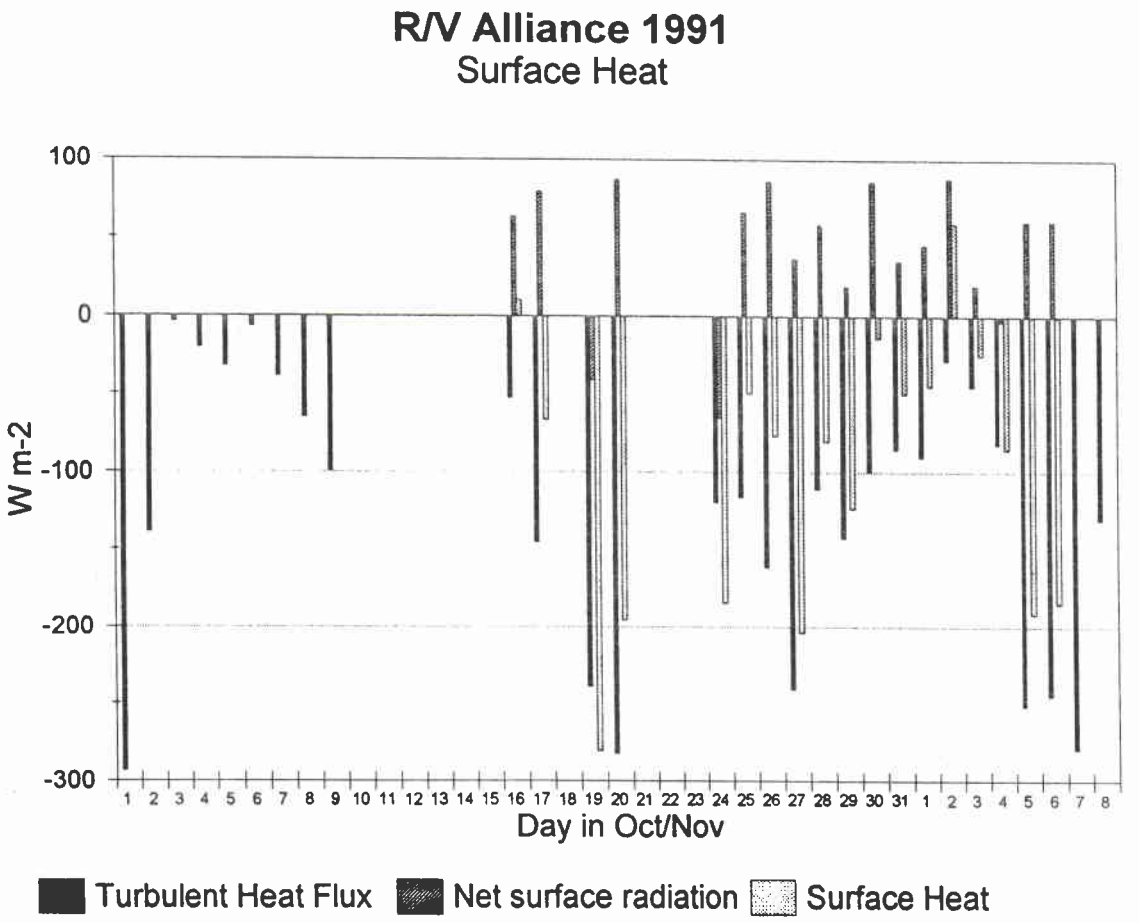

Figure 6 *Bar chart of the daily mean values of the turbulent air–sea heat fluxes, net surface radiation and resultant surface heat budget. Negative values indicate heat loss by the ocean.*

References

Beer, T. (1990). Applied Environmetrics Meteorological Tables, version 1.11. Balwyn, Victoria, Australia, Applied Environmetrics. [ISBN 0 9590809 1 0]

Grant, W.B. (1990). Water vapor absorption coefficients in the 8–13μm spectral region: a critical review. *Applied Optics*, **26**, 451–462.

Grimmer, R.P. (1990). Pyrgeometer calibration. MRF Technical Note 4. Unpublished report of the Meteorological Research Flight. Farnborough, U.K., Royal Aerospace Establishment, 15pp.

Llewellyn-Jones, D.T., Minnett, P.J., Saunders, R.W. and Zavody, A.M. (1984). Satellite multichannel infrared measurements of sea-surface temperature of the N.E. Atlantic Ocean using AVHRR/2. *Quarterly Journal of the Royal Meteorological Society*, **110**, 613–631.

MacWhorter, M. A. and Weller, R.A. (1991). Error in measurements of incoming shortwave radiation made from ships and buoys. *Journal of Atmospheric and Oceanic Technology*, **8**, 108–117.

Minnett, P.J. (1986). A numerical study of the effects of anomalous North Atlantic atmospheric conditions on the infrared measurement of sea-surface temperature from space. *Journal of Geophysical Research*, **91**, 8509–8521.

Minnett, P.J. (1990). The regional optimization of infrared measurements of sea-surface temperature from space. *Journal of Geophysical Research*, **95**, 13,497–13,510.

Minnett P.J. (1992). Surface measurements made from the RV *Alliance* during the Mediterranean Aircraft–Ship Transmission Experiment (MASTEX), June 1990, SACLANTCEN SM-264. La Spezia, Italy, SACLANT Undersea Research Centre.

Minnett P.J. and Saunders, R.W. (1989). Validation of spaceborne radiometers: co-ordinated ship and aircraft measurements. Proceedings of Fourth European AVHRR Data Users Meeting, EUM P 06. Darmstadt-Eberstadt, Federal Republic of Germany, EUMETSAT. pp. 329–334.

Payne, R. (1972). Albedo of the sea surface. *Journal of the Atmospheric Sciences*, **29**, 959–970.

Reynolds, R.M., Hendershot, R., Jungck, M. and Reid, B. (1988). The ZENO Alliance Network: a dual-loop fiber optic instrumentation network for ships. *In*: Institute of Electrical and Electronics Engineers. Oceanic Engineering Society. Oceans '88. Baltimore, MD. Piscataway, NJ, IEEE, 1988. pp. 113–123.

Robinson, I.S., Wells, N.C. and Charnock, H. (1984). The sea surface thermal boundary layers and its relevance to the measurement of sea surface temperature by airborne and spaceborne radiometers. *International Journal of Remote Sensing*, **5**, 19–46.

Saunders R.W. and Minnett, P.J. (1990). Ship and aircraft measurements for the validation of spaceborne radiometers and radiative transfer models. EOS, *Transactions of the American Geophysical Union*, **71**, 157. (Abstract only).

Schluessel, P., Shin, H-Y., Emery, W.J. and Grassl, H. (1987). Comparison of satellite–derived sea-surface temperatures with *in situ* skin measurements. *Journal of Geophysical Research*, **92**, 2859–2874.

Smith, S.D. (1988). Coefficients for sea surface wind stress, heat flux, and wind profiles as a function of wind speed and temperature. *Journal of Geophysical Research*, **93**, 15,467–15,472.

Strong, A.E. and McClain, E.P. (1984). Improved ocean surface temperatures from space – comparisons with drifting buoys. *Bulletin of the American Meteorological Society*, **85**, 138–142.

Initial Distribution for SM-273

SCNR for SACLANTCEN	
SCNR Belgium	1
SCNR Canada	1
SCNR Denmark	1
SCNR Germany	1
SCNR Greece	1
SCNR Italy	1
SCNR Netherlands	1
SCNR Norway	1
SCNR Portugal	1
SCNR Spain	1
SCNR Turkey	1
SCNR UK	1
SCNR US	2
French Delegate	1
SECGEN Rep. SCNR	1
NAMILCOM Rep. SCNR	1

National Liaison Officers	
NLO Belgium	1
NLO Canada	1
NLO Denmark	1
NLO Germany	1
NLO Italy	1
NLO Netherlands	1
NLO UK	3
NLO US	4

Total external distribution	30
SACLANTCEN Library	10
Stock	20
Total number of copies	60